

I N S T I T U T   D ' A E R O N O M I E   S P A T I A L E   D E   B E L G I Q U E

3 - Avenue Circulaire

B - 1180 BRUXELLES

## AERONOMICA ACTA

A - N° 117 - 1973

Nitric acid vapor absorption cross-section spectrum  
and its photodissociation in the stratosphere

by

F. BIAUME

B E L G I S C H   I N S T I T U U T   V O O R   R U I M T E - A E R O N O M I E

3 - Ringlean

B - 1180 BRUSSEL

## FOREWORD

This paper has been submitted for publication to the Journal of Photochemistry and will soon appear in this review.

## AVANT-PROPOS

Cet article a été soumis au "Journal of Photochemistry" en vue de la publication et paraîtra prochainement dans cette revue.

## VOORWOORD

Deze tekst werd voor publicatie aan het "Journal of Photochemistry" gezonden en zal binnenkort daarin verschijnen.

## VORWORT

Dieser Text wurde zum "Journal of Photochemistry" eingegeben und wird in diese Zeitschrift herausgegeben werden.

# NITRIC ACID VAPOR ABSORPTION CROSS SECTION SPECTRUM AND ITS PHOTODISSOCIATION IN THE STRATOSPHERE

by

F. BIAUME

## *Abstract*

Absorption cross section values of nitric acid vapor at room temperature have been measured at different wavelengths in the 1850 Å - 3250 Å spectral range. In conjunction with recently published data, they lead to a precise  $\text{HNO}_3$  absorption curve. Estimates, assuming a quantum yield equal to unity, are also given for the nitric acid photodissociation coefficient in the stratosphere.

## *Résumé*

Des valeurs de la section efficace d'absorption de la vapeur d'acide nitrique à la température ordinaire ont été mesurées à différentes longueurs d'onde dans le domaine spectral de 1850 Å à 3250 Å. En accord avec des données publiées récemment, ces résultats conduisent à une courbe d'absorption très précise. Des estimations, basées sur l'hypothèse d'un rendement quantique unitaire, sont également données pour le coefficient de photodissociation de l'acide nitrique dans la stratosphère.

### *Samenvatting*

Verschillende waarden van de werkzame absorptiedoorsnede voor salpeterzuurdamp bij kamertemperatuur werden gemeten voor meerdere golflengten in het gebied van 1850 Å tot 3250 Å. Uit deze metingen en onlangs gepubliceerde gegevens, werd een juiste absorptiecurve afgeleid. In de veronderstelling dat de quantum opbrengst één is, werden waarden berekend voor de fotodissociatie-coëfficiënt van  $\text{HNO}_3$  in de stratosfeer.

### *Zusammenfassung*

Absorptionsdurchschnitte für Salpersäuredampf wurden bei verschiedenen Wellenlängen zwischen 1850 Å und 3250 Å für Raumtemperatur gemessen. Diese Ergebnisse und verschiedene herausgegebene Resultaten leiten zu einer genauen Absorptionskurve. Mit einer Quantenausbeute von 1, wird der Photodissoziationskoeffizient von  $\text{HNO}_3$  in der Stratosphäre berechnet.

## INTRODUCTION

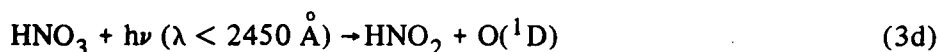
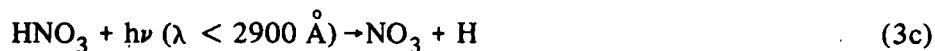
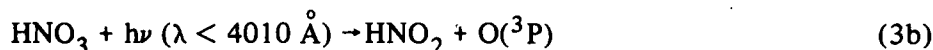
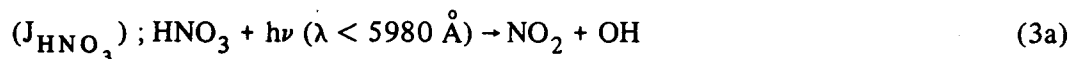
Nitric acid, which has recently been observed in the stratosphere by Murcray *et al*<sup>1, 2</sup> is related to the nitrogen oxides<sup>3</sup>. An accurate determination of its stratospheric distribution is thus necessary to estimate the behavior of minor constituents such as nitrogen dioxide and hydroxyl radical<sup>4</sup>. Nitric acid is produced by the reaction



and is destroyed by the two-body reaction



or in a sunlit atmosphere, by photodissociation processes<sup>5, 6</sup>



The nitric acid concentration is thus very sensitive to the OH profile and to the vertical distribution of the photodissociation mechanisms. Therefore, precise measurements of the HNO<sub>3</sub> absorption cross section are required in the UV spectral range where the photodissociation takes place.

Since the pioneer work of Dalmon<sup>7</sup> only two measurements of the nitric acid UV absorption spectrum by Schmidt *et al*<sup>8</sup> and by Johnston and Graham<sup>6</sup>, have been made. This paper reports measurements at the wavelengths of 37 atomic lines in the 1850 Å - 3650 Å spectral range. Using these new data, the nitric acid photodissociation coefficient is presented for different wavelength intervals and various altitudes. The results show two

large spectral contributions which are situated in the 2000 Å atmospheric window and at  $\lambda > 3000$  Å. According to (3a), (3b), (3c) and (3d), they may represent different dissociation processes.

### *EXPERIMENTAL*

The instrumentation used in this study has already been described in detail<sup>9, 10</sup>. Briefly, it consisted of a 50 cm focal length Bausch and Lomb grating monochromator in conjunction with a 400,5 cm length absorption cell and an EMI 6255 Mg photomultiplier. The absorption cell, sealed at each end with a "suprasil" quartz lens, was connected to a gas handling system provided with reservoirs, traps and manometers. The whole system, which could be evacuated down to  $10^{-6}$  Torr, was constructed in pyrex and equipped with silicone greased stopcocks.

The nitric acid was prepared by molecular distillation at low temperature and in the dark in order to prevent thermal and photodecomposition. High purity  $\text{HNO}_3$  was distilled under vacuum ( $10^{-5}$  Torr) from a bulb containing a (40 %  $\text{HNO}_3$  at min. 65% and 60%  $\text{H}_2\text{SO}_4$  at min. 96% ; Merck Darmstadt, FRG) sulfonitric mixture maintained at  $0^\circ\text{C}$  into a trap cooled at liquid nitrogen temperature. This procedure was followed by several successive distillations from trap to trap at  $0^\circ\text{C}$  and  $-196^\circ\text{C}$  respectively in order to remove evacuable impurities like  $\text{N}_2$  and  $\text{O}_2$ . The product was finally stored as a white crystalline solid at liquid nitrogen temperature in a reservoir closed by a greaseless teflon O-ring stopcock.

Since nitric acid has a continuous absorption, the measurements were made at the different line wavelengths emitted by a  $\text{SiCl}_4$  microwave lamp<sup>11</sup> and by Hg, Cd, Zn and Hg discharge lamps manufactured by Philips. The lines of proper wavelength were selected in the first order of the monochromator and their light intensity was measured by the photomultiplier after passage through the absorption cell which was either evacuated or filled with the nitric acid vapor at various pressures.

For each absorption measurement in the 2000 Å to 3000 Å region nitric acid was warmed up to  $0^\circ\text{C}$  and the gas phase was introduced into the absorption cell at pressures

varying from  $\sim 0$  to 14 Torr. At wavelengths larger than  $3000 \text{ \AA}$ , the reservoir containing the acid was warmed up to the room temperature in order to obtain a measurable absorption by the use of pressures, up to 45 Torr. On the contrary, very low pressures were needed at wavelengths below  $2000 \text{ \AA}$ , as the absorption of nitric acid increases importantly. In these conditions, different gas samples were collected in a small section of the gas handling system and then expanded into the absorption cell. The volume ratio  $\left(\frac{v}{v+V} = 2.096 \cdot 10^{-2}\right)$  between the gas handling system and the cell was established experimentally by two absorption measurements at  $2124,1 \text{ \AA}$  realised by direct introduction and by expansion of the gas respectively. Pressure measurements in excess of 14 Torr were made by means of a Bourdon gauge balanced by air pressure read on a mercury manometer ; a silicone oil manometer read with a cathetometer was used for lower values.

### RESULTS AND DISCUSSION

The absorption cross section values obtained at various wavelengths were deduced from the experimental data according to the Beer's law expression

$$\sigma_{\lambda} = \left[ n_o \frac{P}{P_o} \cdot \frac{T_o}{T} \cdot d \right]^{-1} \times 2.303 \log_{10} \frac{I_o}{I} \quad (4)$$

where  $\sigma_{\lambda} \text{ (cm}^2\text{)}$  is the absorption cross section ;  $n_o \text{ (} 2.6872 \times 10^{19} \text{ part. cm}^{-3}\text{)}$  is Loschmidt number ;  $P_o \text{ (760 Torr)}$  and  $T_o \text{ (273.16}^\circ\text{K)}$  are respectively the pressure and temperature in standard conditions ;  $d \text{ (400.5 cm)}$  is the pathlength used and  $\log_{10} \frac{I_o}{I}$  corresponds to the observed optical density.

This linear relation (4) can be applied (see fig. 1 and 2) to the measurements which did not require nitric acid vapor pressure exceeding 20 Torr in the 400.5 cm absorption cell which is used here. It is also the case for every measurement performed at shorter wavelengths than  $3200 \text{ \AA}$  where the absorption cross section is not too small.

A systematic departure from Beer's law was observed for the other measurements ; it is shown in fig. 3 and characterized by a non linear increase of the optical density above a certain pressure ( $\sim 25$  Torr). This departure could be due either to condensation on the windows of the absorption cell - as the acid contained in the storage reservoir must be

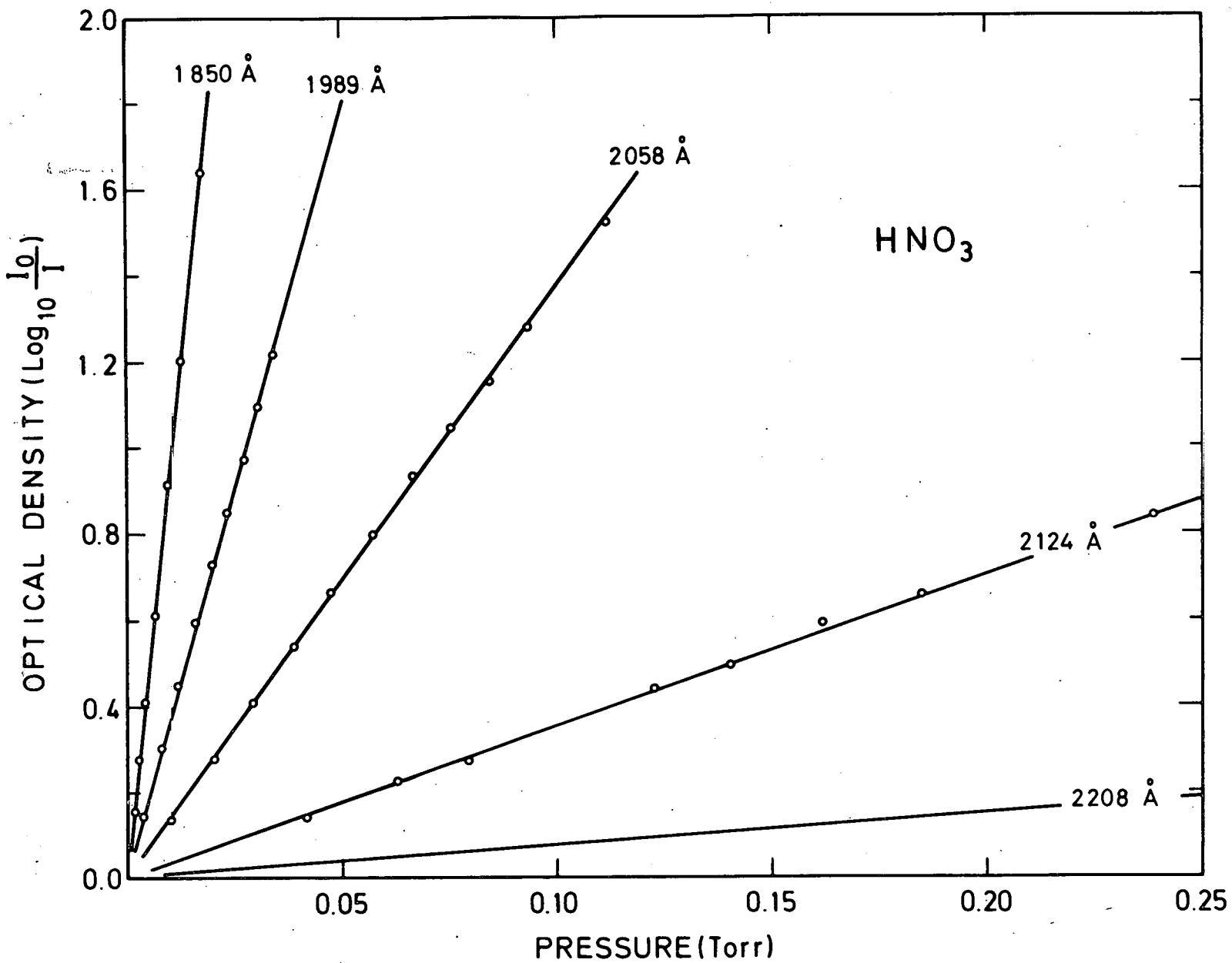


Fig. 1.- Nitric acid optical density versus pressure for various wavelengths in the 1850 Å - 2200 Å spectral range.



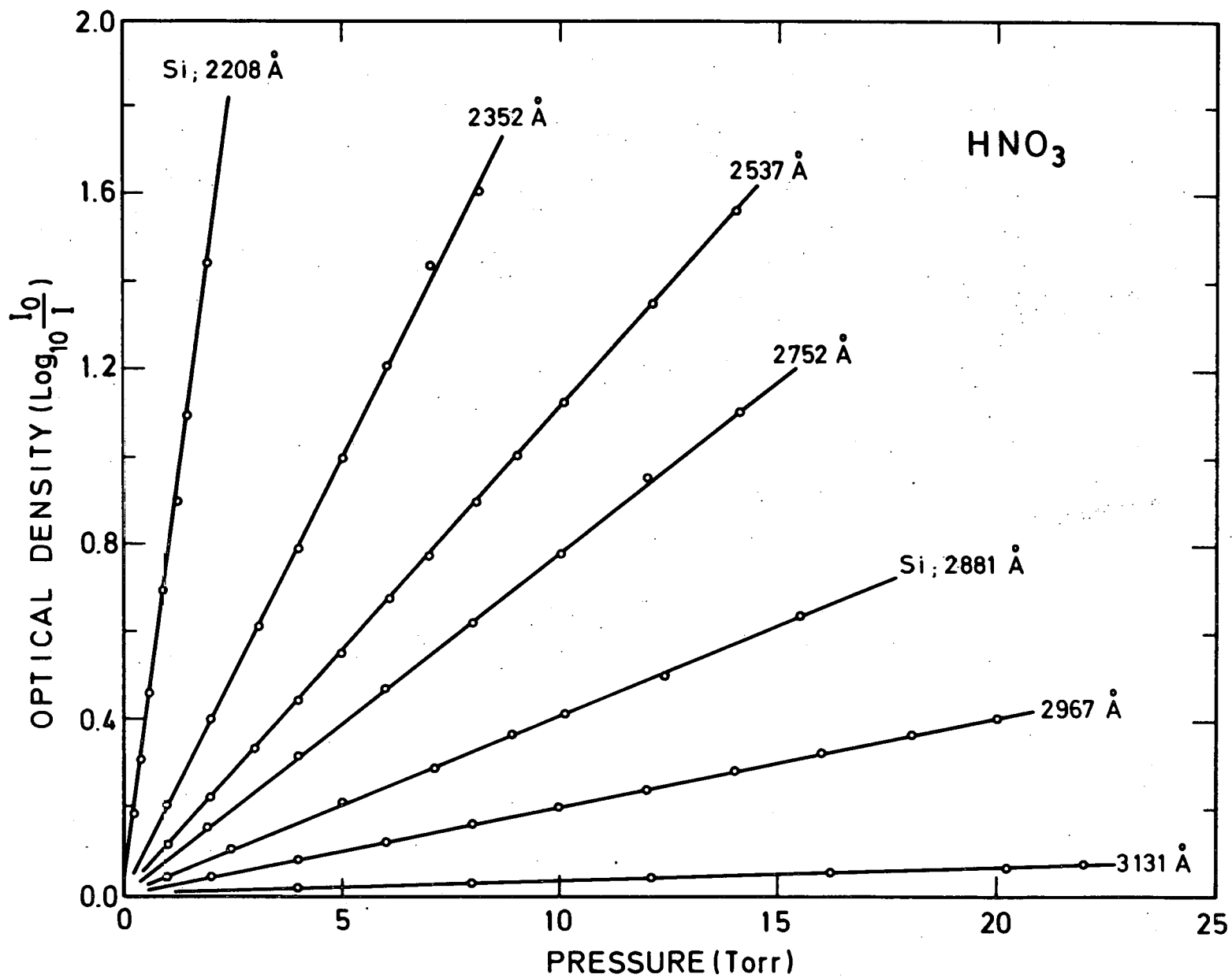


Fig. 2.- Nitric acid optical density versus pressure for various wavelengths in the 2200 Å - 3100 Å spectral range.

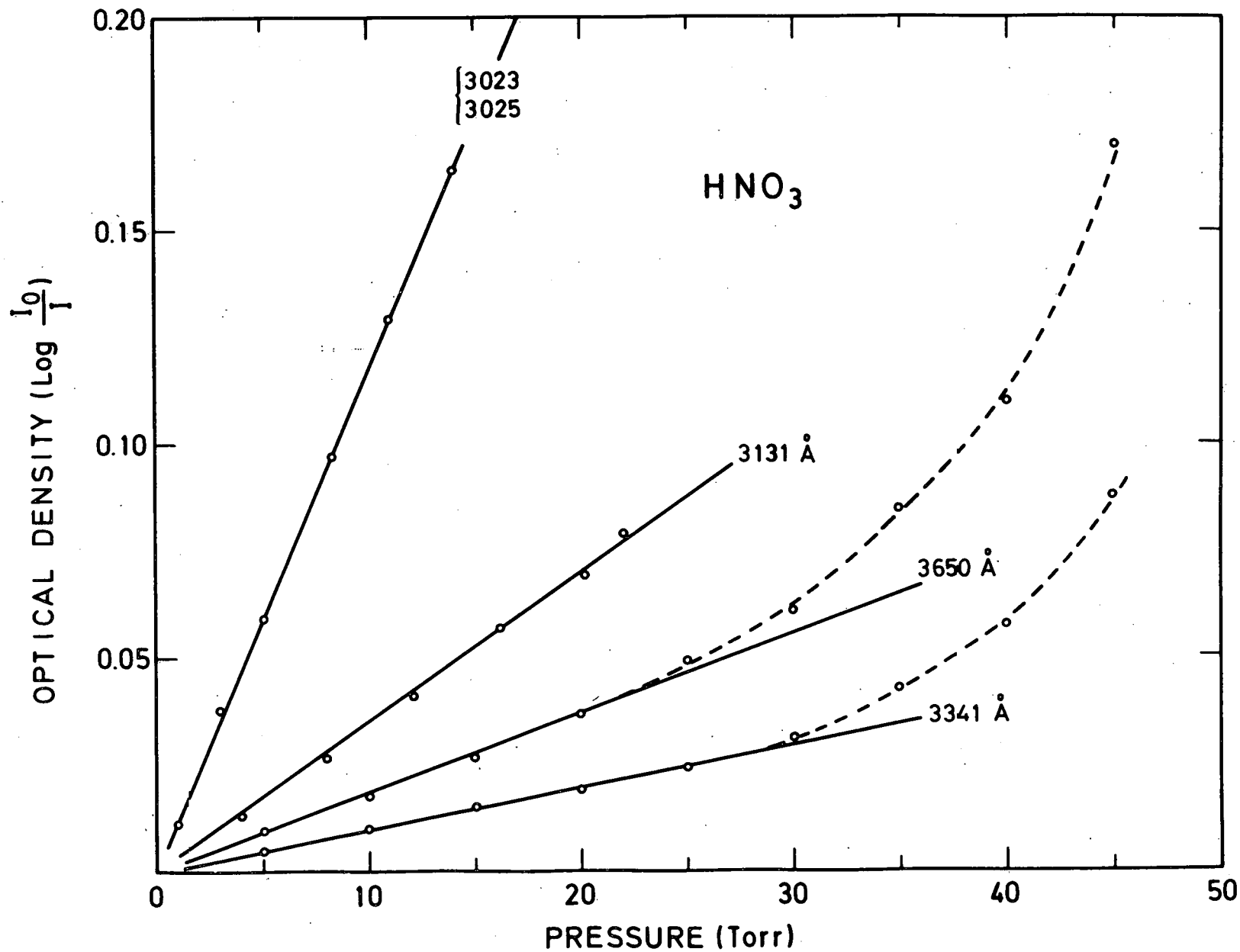


Fig. 3.- Nitric acid optical density versus pressure for various wavelengths in the 3000 Å - 3650 Å spectral range. The departure from Beer's law appears above 20 Torr, for the measurements at 3341 Å and 3650 Å.

warmed to get rapidly needed pressure - either to nitrogen oxides formed by thermal decomposition or by reaction of  $\text{HNO}_3$  with the silicone grease of the stopcocks. In these particular cases, the absorption cross section values were determined from the linear portions of the optical density curves presented in fig. 3.

In order to detect traces of nitrogen dioxide in the nitric acid, absorption measurements were made in the 3300 Å - 3650 Å spectral range assuming that nitric acid does not practically absorb at those wavelengths<sup>6</sup>. A concentration ratio  $[\text{NO}_2]/[\text{HNO}_3]$  of about  $(4.5 \pm 0.5) \times 10^{-4}$  was found comparing the experimental results (see fig. 4) with the  $\text{NO}_2$  absorption curve of Hall and Blacet<sup>12</sup>. From 3000 Å to 3250 Å, the absorption contribution due to  $\text{NO}_2$ , deduced from this curve, was taken into account in the experimental results. No correction for nitrogen tetroxide absorption was made, since in the present experiments, the maximum value of the  $[\text{N}_2\text{O}_4]/[\text{NO}_2]$  relative concentration estimated from the  $\text{N}_2\text{O}_4 \rightleftharpoons 2 \text{NO}_2$  equilibrium constant of Verhoek and Daniels<sup>13</sup>, would be of the order of  $3 \times 10^{-4}$ .

The absorption cross section values are given in Table I. Probable experimental errors are estimated to  $\pm 3\%$  in the 1850 Å - 2100 Å region,  $\pm 1\%$  in the 2100 Å - 3000 Å region and about  $\pm 10\%$  above 3000 Å. Fig. 5 represents the best fit curve throughout the experimental points and shows the  $\text{NO}_2$  absorption contribution above 3000 Å. Excellent agreement appears in this figure with the recent measurements of Johnston and Graham<sup>6</sup>. Only slight differences exist at both end of the absorption curve where the experimental errors are the largest. However, the value of  $2 \times 10^{-23} \text{ cm}^2$  adopted by these authors at 3250 Å seems to be somewhat low and could be due to an overestimation of the  $\text{NO}_2$  quantity present in their  $\text{HNO}_3$ . Nevertheless, as it will be shown below, this discrepancy could not play an important role in aeronomic applications.

### *NITRIC ACID STRATOSPHERIC PHOTODISSOCIATION*

In order to estimate the aeronomic implications of the  $\text{HNO}_3$  absorption in the UV spectral range, the averaged absorption cross section values listed in Table II have been adopted to each wavenumber interval of the solar flux used by Ackerman<sup>14</sup>. Assuming a quantum yield equal to unity<sup>15</sup> the nitric acid photodissociation coefficient  $J_{\text{HNO}_3}$  has then been computed according to the formula :

TABLE I : Absorption cross sections of nitric acid vapor

| Line wavelength<br>(Å) Element | Cross section<br>(cm <sup>2</sup> ) | Line wavelength<br>(Å) Element | Cross section<br>(cm <sup>2</sup> ) |
|--------------------------------|-------------------------------------|--------------------------------|-------------------------------------|
| 1849.9 Hg                      | 1.63 x 10 <sup>-17</sup>            | 2698.9 Hg                      | 1.64 x 10 <sup>-20</sup>            |
| 1942.3 "                       | 1.16                                | 2699.5 "                       |                                     |
| 1988.9 Si                      | 6.19 x 10 <sup>-18</sup>            | 2752.2 "                       | 1.36                                |
| 2058.1 "                       | 2.39                                | 2758.8 "                       |                                     |
| 2124.1 "                       | 6.12 x 10 <sup>-19</sup>            | 2803.5 "                       | 1.09                                |
| 2207.9 "                       | 1.32                                | 2804.5 "                       |                                     |
| 2216.6 "                       | 1.20                                | 2881.6 Si                      | 7.15 x 10 <sup>-21</sup>            |
| 2218.0 "                       |                                     | 2893.6 Hg                      | 6.42                                |
| 2302.1 Hg                      | 5.35 x 10 <sup>-20</sup>            | 2967.3 "                       | 3.57                                |
| 2352.5 "                       | 3.49                                | 2967.6 "                       |                                     |
| 2378.3 "                       | 2.97                                | 3023.5 "                       | 2.06 *                              |
| 2399.4 "                       | 2.61                                | 3025.6 "                       |                                     |
| 2399.7 "                       |                                     | 3131.5 "                       | 6.02 x 10 <sup>-22</sup> *          |
| 2435.1 Si                      | 2.15                                | 3131.8 "                       |                                     |
| 2484.8 Hg                      | 1.98                                | 3252.5 Cd                      | 2.09 *                              |
| 2506.9 Si                      | 1.94                                | 3341.5 Hg                      | 1.71                                |
| 2514.3 "                       | 1.94                                | 3403.6 Cd                      | 2.33                                |
| 2516.1 "                       |                                     | 3466.2 "                       | 2.13                                |
| 2519.2 "                       | 1.94                                | 3612.9 "                       | 2.44                                |
| 2524.1 "                       | 1.94                                | 3650.1 Hg                      | 3.20                                |
| 2528.5 "                       | 1.94                                |                                |                                     |
| 2532.3 "                       | 1.94                                | 3023.5 Hg                      | 1.98 x 10 <sup>-22</sup>            |
| 2536.5 Hg                      | 1.95                                | 3025.6 "                       |                                     |
| 2576.3 "                       | 1.93                                | 3131.5 "                       | 4.9                                 |
| 2631.2 Si                      | 1.81                                | 3131.8 "                       |                                     |
| 2652.0 Hg                      | 1.77                                | 3252.5 Cd                      | 6.0 x 10 <sup>-23</sup>             |

(\*) These values include the NO<sub>2</sub> absorption contribution. The corrected values are listed at the end of the Table.

TABLE II : Averaged absorption cross section values for nitric acid vapor

| Wavenumber interval (cm <sup>-1</sup> ) | Wavelength interval (Å) | Averaged cross section (cm <sup>2</sup> ) | Wavenumber interval (cm <sup>-1</sup> ) | Wavelength interval (Å) | Averaged cross section (cm <sup>2</sup> ) |
|---|-------------------------|---|---|-------------------------|---|
| 54000-53500                             | 1852-1869               | 1.62 x 10 <sup>-17</sup>                  | 41000-40500                             | 2439-2469               | 2.05 x 10 <sup>-20</sup>                  |
| 53500-53000                             | 1869-1887               | 1.58                                      | 40500-40000                             | 2469-2500               | 1.97                                      |
| 53000-52500                             | 1887-1905               | 1.47                                      | 40000-39500                             | 2500-2532               | 1.94                                      |
| 52500-52000                             | 1905-1923               | 1.37                                      | 39500-39000                             | 2532-2564               | 1.94                                      |
| 52000-51500                             | 1923-1942               | 1.21                                      | 39000-38500                             | 2564-2597               | 1.92                                      |
| 51500-51000                             | 1942-1961               | 1.01                                      | 38500-38000                             | 2597-2632               | 1.86                                      |
| 51000-50500                             | 1961-1980               | 8.00 x 10 <sup>-18</sup>                  | 38000-37500                             | 2632-2667               | 1.78                                      |
| 50500-50000                             | 1980-2000               | 6.50                                      | 37500-37000                             | 2667-2703               | 1.67                                      |
| 50000-49500                             | 2000-2020               | 4.81                                      | 37000-36500                             | 2703-2740               | 1.52                                      |
| 49500-49000                             | 2020-2041               | 3.56                                      | 36500-36000                             | 2740-2778               | 1.34                                      |
| 49000-48500                             | 2041-2062               | 2.46                                      | 36000-35500                             | 2778-2817               | 1.14                                      |
| 48500-48000                             | 2062-2083               | 1.71                                      | 35500-35000                             | 2817-2857               | 9.29 x 10 <sup>-21</sup>                  |
| 48000-47500                             | 2083-2105               | 1.12                                      | 35000-34500                             | 2857-2899               | 7.15                                      |
| 47500-47000                             | 2105-2128               | 7.56 x 10 <sup>-19</sup>                  | 34500-34000                             | 2899-2941               | 5.33                                      |
| 47000-46500                             | 2128-2150               | 4.66                                      | 34000-33500                             | 2941-2985               | 3.65                                      |
| 46500-46000                             | 2150-2174               | 3.21                                      | 33500-33000                             | 2985-3030               | 2.41                                      |
| 46000-45500                             | 2174-2198               | 2.07                                      | 33000-32500                             | 3030-3077               | 1.45                                      |
| 45500-45000                             | 2198-2222               | 1.35                                      | 32500-32000                             | 3100 ± 25               | 7.86 x 10 <sup>-22</sup>                  |
| 45000-44500                             | 2222-2247               | 9.70 x 10 <sup>-20</sup>                  | 32000-31496                             | 3150                    | 3.75                                      |
| 44500-44000                             | 2247-2273               | 7.53                                      | 31496-31008                             | 3200                    | 1.62                                      |
| 44000-43500                             | 2273-2299               | 6.00                                      | 31008-30534                             | 3250                    | 6.50 x 10 <sup>-23</sup>                  |
| 43500-43000                             | 2299-2326               | 4.98                                      | 30534-30075                             | 3300                    | 2.60 *                                    |
| 43000-42500                             | 2326-2353               | 4.03                                      | 30075-29630                             | 3350                    | 1.03 *                                    |
| 42500-42000                             | 2353-2381               | 3.25                                      | 29630-29197                             | 3400                    | 4.10 x 10 <sup>-24</sup> *                |
| 42000-41500                             | 2381-2410               | 2.64                                      | 29197-28777                             | 3450                    | 1.60 *                                    |
| 41500-41000                             | 2410-2439               | 2.29                                      |   |                         |   |

(\*) Extrapolated values.

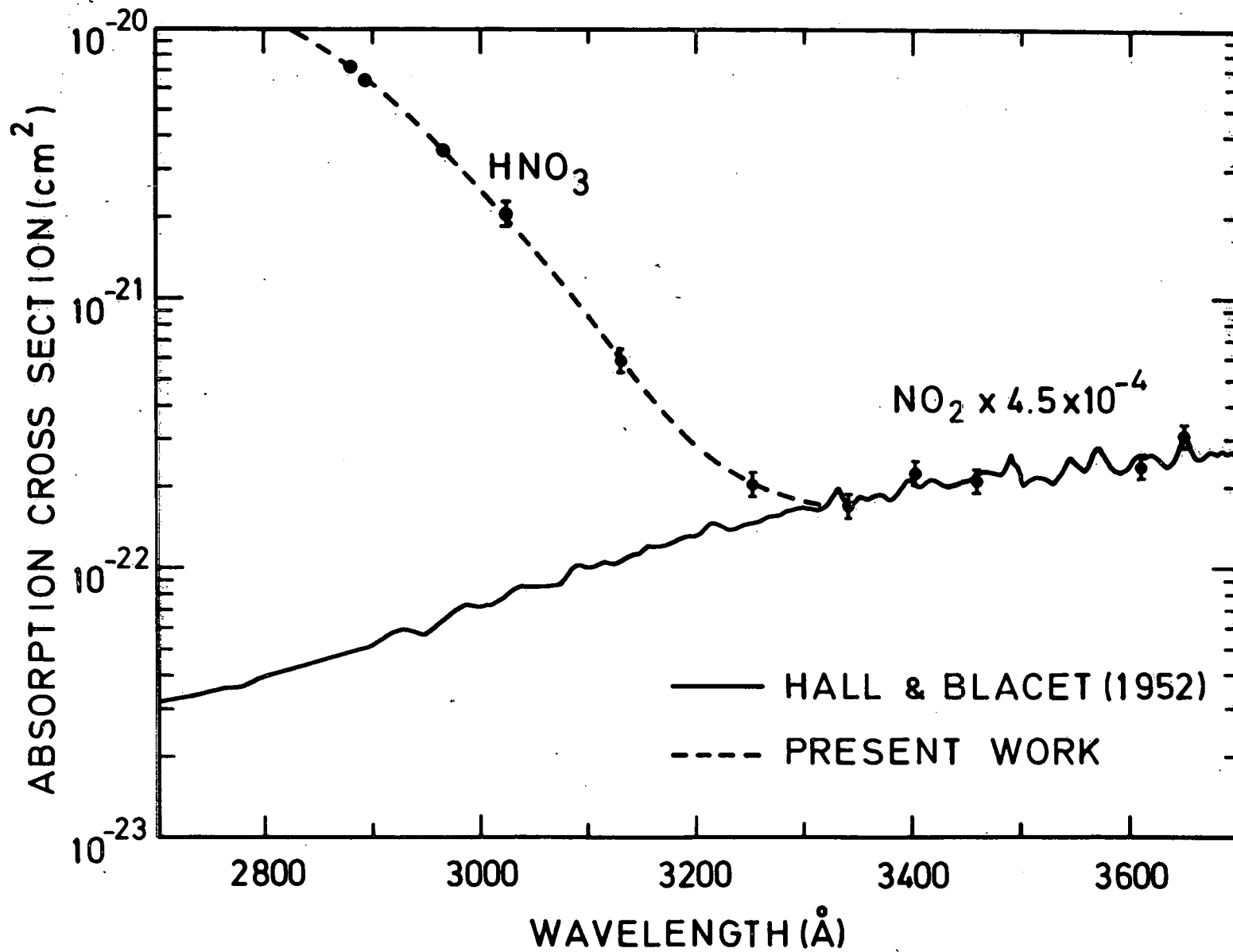


Fig. 4.- Absorption cross section measurements in the 2700 Å - 3700 Å spectral range. The contribution due to nitrogen dioxide above 3250 Å is shown by Hall and Blacet's NO<sub>2</sub> absorption curve which is multiplied by 4.5 x 10<sup>-4</sup> in order to fit our experimental results.

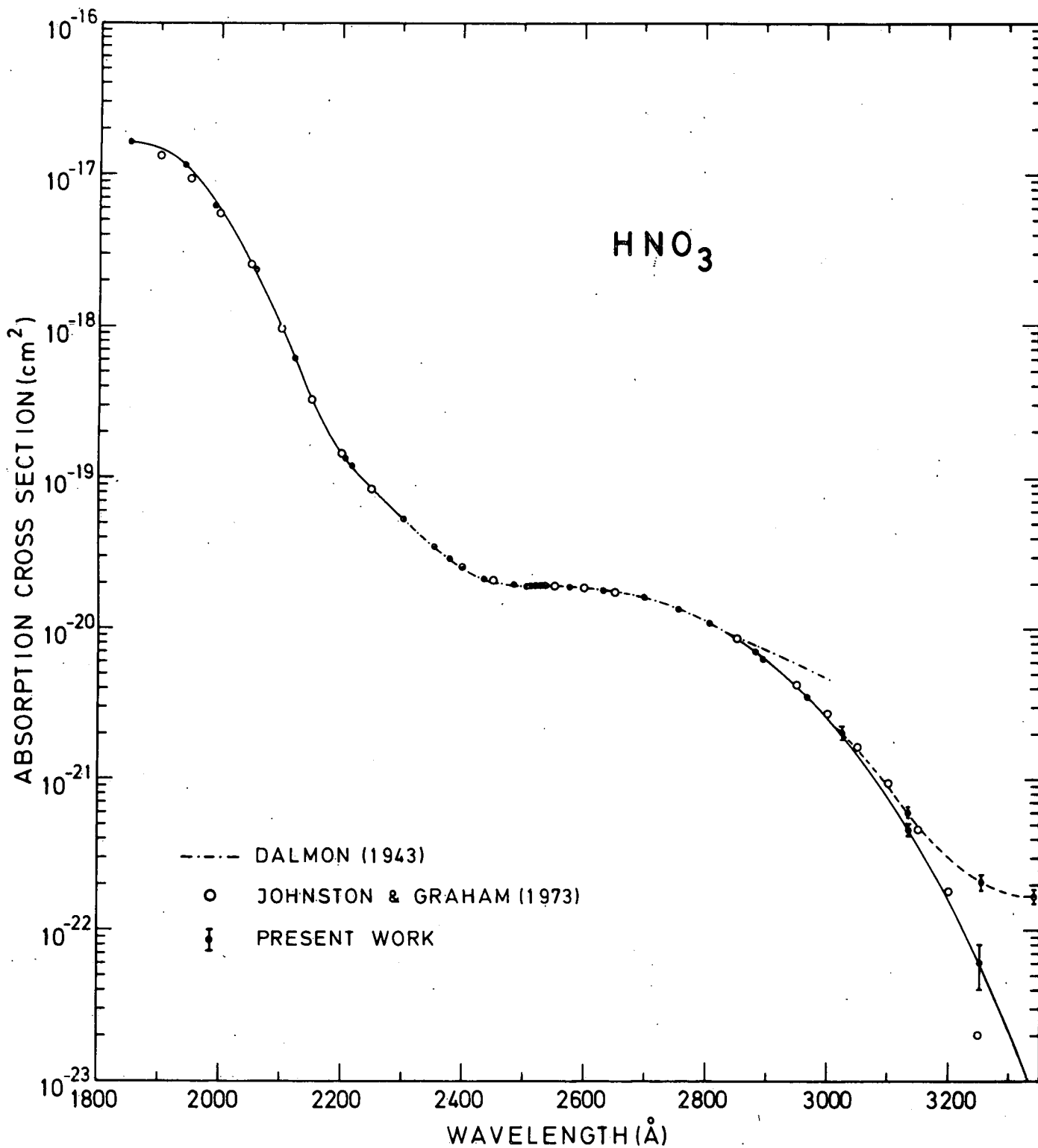


Fig. 5.- Nitric acid absorption cross section measurements in the 1850 Å - 3350 Å spectral range. The very good agreement between the present results and the recent data of Johnston and Graham leads to an accurate  $\text{HNO}_3$  UV absorption curve.

$$J_{\text{HNO}_3} = \sum_{\Delta\nu_i} \sigma_{\text{HNO}_3}(\Delta\nu_i) \times \Phi_z(\Delta\nu_i) \quad (5)$$

where  $\sigma_{\text{HNO}_3}(\Delta\nu_i)$ , ( $\text{cm}^2$ ) and  $\Phi_z(\Delta\nu_i)$ , ( $\text{cm}^{-2}, \text{s}^{-1}$ ) are respectively the  $\text{HNO}_3$  absorption cross section and the solar flux at altitude  $z$ , averaged in the same wavenumber interval  $\Delta\nu_i$ .

At the top of the atmosphere (see fig. 6), the photodissociation reaches a maximum near  $2000 \text{ \AA}$  and falls off by more than an order of magnitude towards  $2500 \text{ \AA}$  where the decrease of the  $\text{HNO}_3$  absorption cross section is counterbalanced by the increase of the solar flux. At wavelengths larger than  $3000 \text{ \AA}$  the contribution to  $J_{\text{HNO}_3}$  becomes negligible since the absorption cross section decreases very sharply. An integration over the whole  $1850 \text{ \AA} - 3450 \text{ \AA}$  spectral range leads to a total photodissociation coefficient of  $1.7 \times 10^{-4} \text{ s}^{-1}$  at the top of the atmosphere. This value represents a lower limit as the contribution below  $1850 \text{ \AA}$  still seems to be large<sup>8</sup>. Nevertheless, this contribution can be neglected in the whole stratosphere since the UV solar radiation shorter than  $1850 \text{ \AA}$  is absorbed in the mesosphere by the Schumann-Runge system of molecular oxygen<sup>16, 17</sup>.

The ozone absorption strongly reduces the dissociation rate in the  $2200 \text{ \AA} - 2900 \text{ \AA}$  region. For example, at  $2500 \text{ \AA}$  where the  $\text{O}_3$  absorption reaches a maximum,  $J_{\text{HNO}_3}$  decreases by about two orders of magnitude at  $40 \text{ km}$  if the atmospheric model deduced by Nicolet<sup>18, 19</sup> is adopted for overhead sun conditions. Then, in the stratosphere, two spectral intervals play a major role. The first one, around  $2000 \text{ \AA}$ , is the most important at high altitudes and the second one, at about  $3000 \text{ \AA}$ , becomes dominant in the lower stratosphere, since the absorption of the solar radiation is very weak in this spectral range. In order to illustrate this double effect, the stratospheric  $J_{\text{HNO}_3}$ , calculated for two partial spectral ranges ( $1850 \text{ \AA} - 2500 \text{ \AA}$  and  $2500 \text{ \AA} - 3450 \text{ \AA}$ ), is represented in fig. 7 as well as the total value. This figure clearly shows that nitric acid photodissociation above  $30 \text{ km}$ , is mostly due to the absorption in the  $1850 \text{ \AA} - 2500 \text{ \AA}$  region since the values from curve A are larger than those from curve B by about a factor of 10. This situation is inverted in the lower stratosphere and in the troposphere where the influence of the  $2500 \text{ \AA} - 3450 \text{ \AA}$  radiation becomes dominant.

Finally, the total photodissociation coefficient, calculated for different solar zenith angles, is plotted versus altitude on fig. 8. Its value, depending on different solar conditions is about  $10^{-4} \text{ s}^{-1}$  at the stratopause and slowly decreases to reach  $10^{-6}$  to  $10^{-7} \text{ s}^{-1}$  at the tropopause.



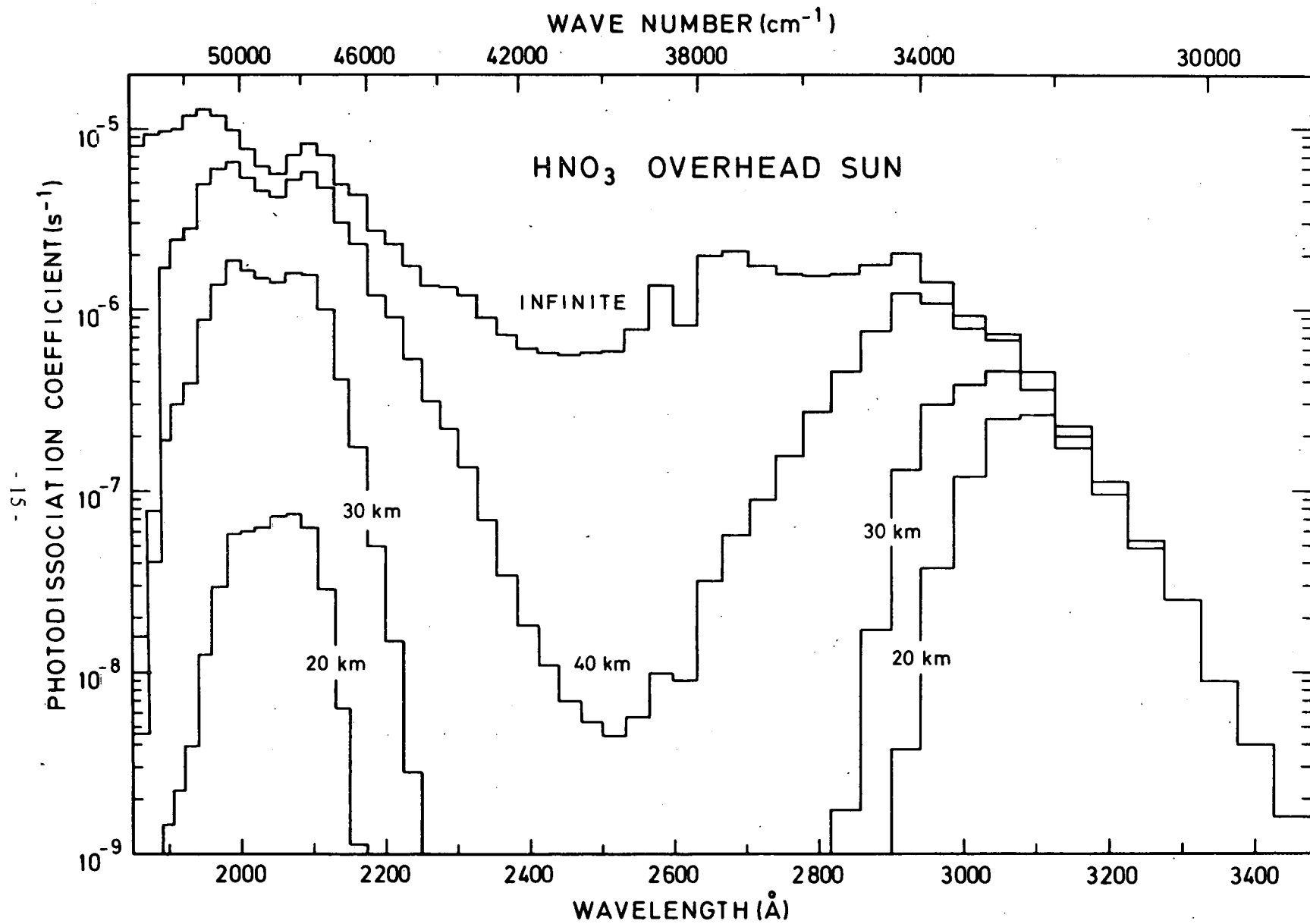


Fig. 6. Nitric acid photodissociation coefficient versus wavelength for overhead sun conditions and various altitudes. The decrease of  $J_{\text{HNO}_3}$  in the  $2200 \text{ \AA} - 2900 \text{ \AA}$  spectral range and below  $2000 \text{ \AA}$  is due to the absorption of the solar flux by stratospheric ozone and by molecular oxygen respectively.

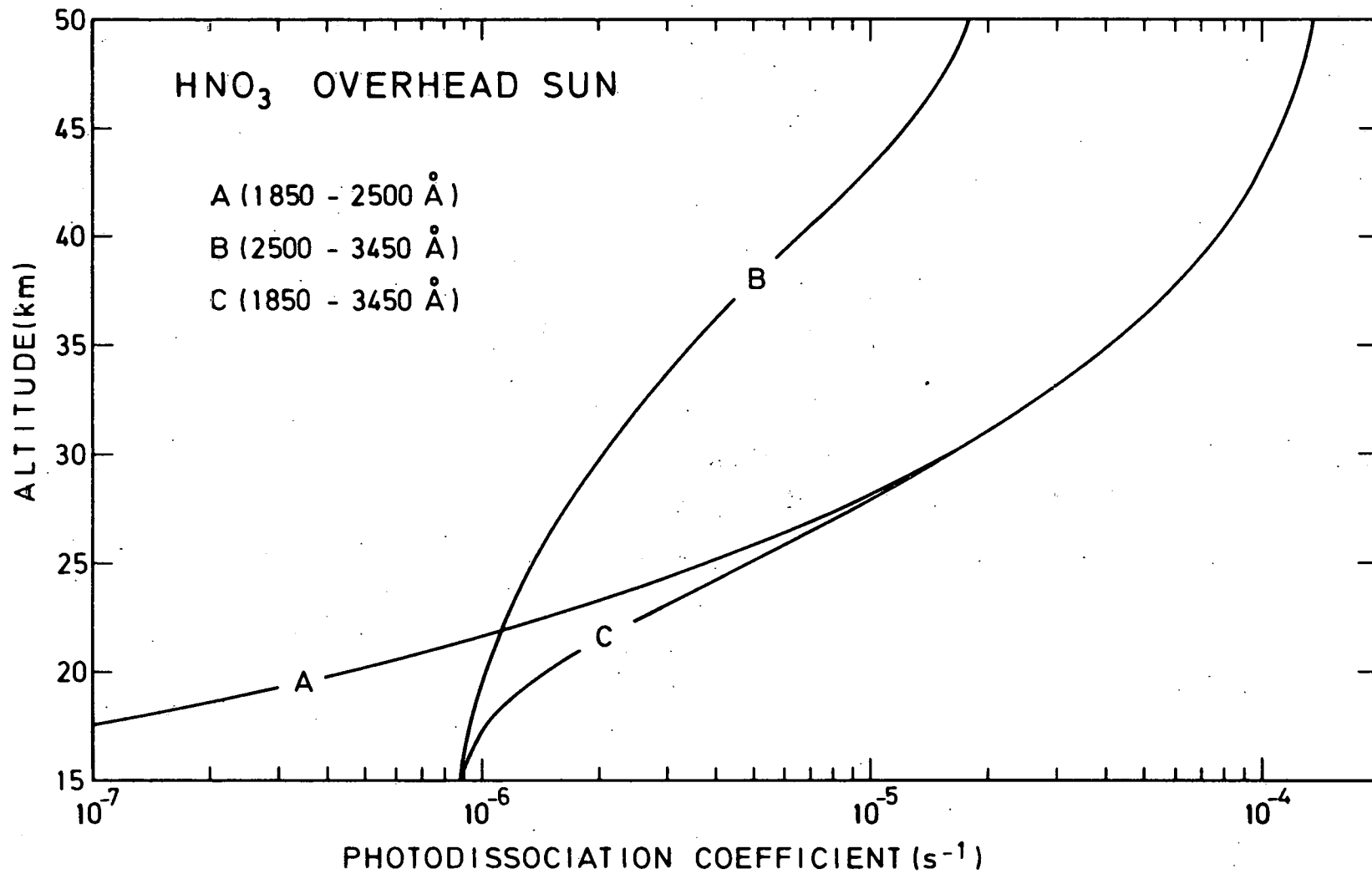


Fig. 7.- Photodissociation coefficient of nitric acid in the stratosphere for two complementary spectral ranges and overhead sun conditions. As shown by curves A, B and C, HNO<sub>3</sub> is mostly dissociated by the short wavelength range of the solar flux in the upper atmosphere and by the long wavelength range in the lower stratosphere.

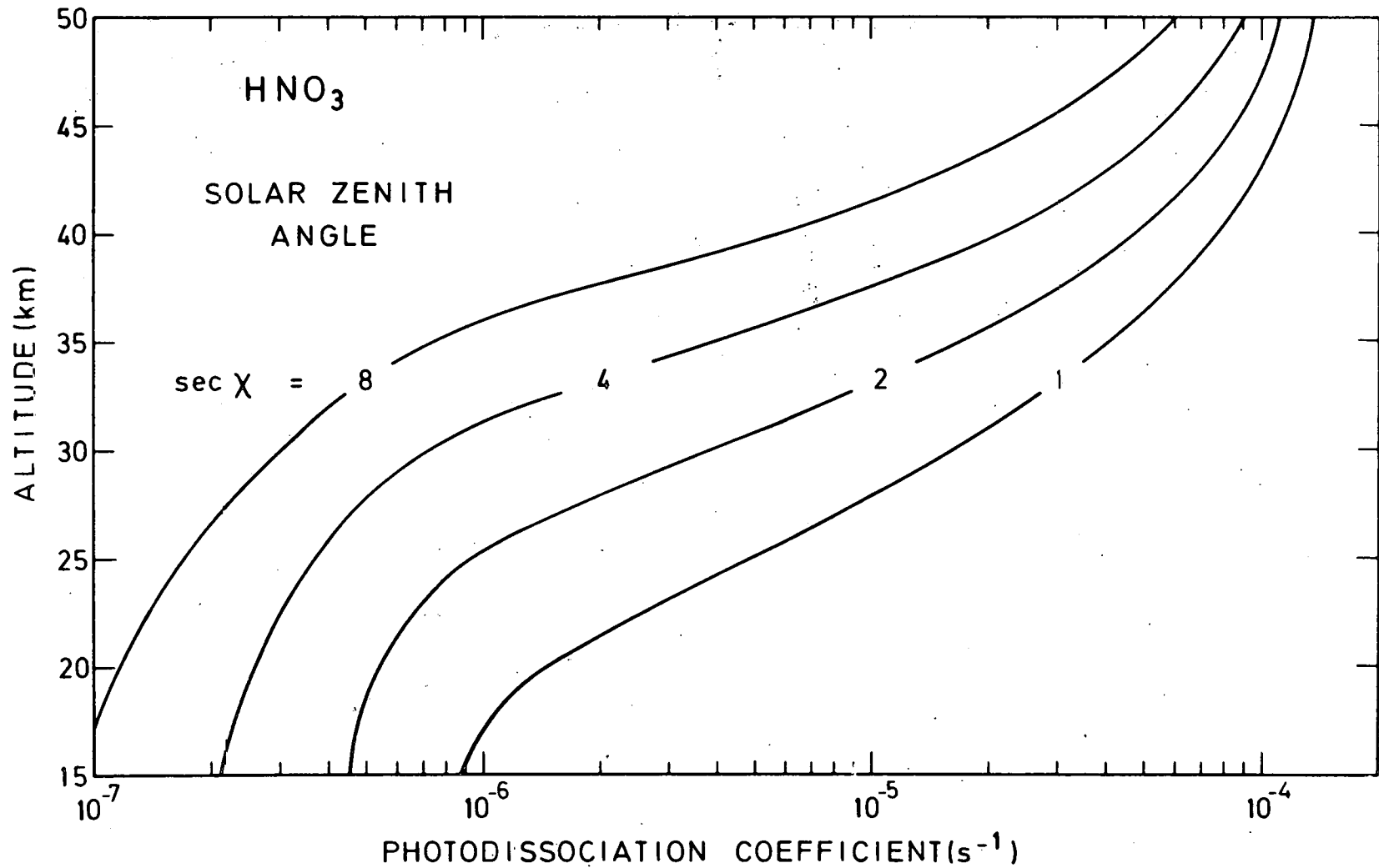


Fig. 8.- Photodissociation coefficient of nitric acid in the stratosphere for various solar zenith angles. From overhead sun conditions,  $\chi = 0^\circ$  to  $\chi = 83^\circ$ .

## CONCLUSIONS

The present absorption cross section measurements are in excellent agreement with the recent data published by Johnston and Graham<sup>6</sup>. They lead to a precise absorption curve from 1850 Å to 3250 Å and confirm the early measurements of Dalmon<sup>7</sup>, over a shorter wavelength interval. The HNO<sub>3</sub> absorption related by Schmidt *et al*<sup>8</sup> could not be detected above 3300 Å, where the contribution of NO<sub>2</sub> cannot be neglected.

The estimate of the nitric acid photodissociation coefficient shows that this loss process is important, but more information concerning the dissociation mechanisms involved in the investigated spectral range is still needed in order to explain the aeronomic behavior of HNO<sub>3</sub> in the lower stratosphere.

## ACKNOWLEDGEMENTS

I am deeply grateful to Professor M. Nicolet for his particular interest and valuable advice during the preparation of this work. I also wish to express my thanks to Mr. G. Brasseur for his useful help and discussions.

## REFERENCES

1. MURCRAY, D.G., KYLE, T.G., MURCRAY, F.H. and WILLIAMS, W.J., *Nature*, **78** (1968) 218.
2. MURCRAY, D.G., KYLE, T.G., MURCRAY, F.H. and WILLIAMS, W.J., *J. Opt. Soc. Am.*, **59** (1969) 1131.
3. NICOLET, M., *J. Geophys. Res.*, **70** (1965) 679.
4. BRASSEUR, G. and NICOLET, M., *Aeronomica Acta A n° 113* (1973), *Planet. Space Sci.* (1973) in press.
5. OKABE, H., Chemical Kinetics Data Survey II, NBS Rept. 10828 (1972).
6. JOHNSTON, H.S. and GRAHAM, R., *J. Phys. Chem.*, **77** (1973) 62.
7. DALMON, R., *Mém. Serv. Chim. Etat*, **30** (1943) 141.
8. SCHMIDT, S.C., AMME, R.C., MURCRAY, D.G., GOLDMAN, A. and BONOMO, F.S., *Nature Phys. Sci.*, **238** (1972) 109.
9. ACKERMAN, M., BIAUME, F. and KOCKARTS, G., *Plan. Space Sc.*, **18** (1970) 1639.
10. BIAUME, F., Thèse de doctorat ULB Mars 1972 *Aeronomica Acta A n° 100* (1972).
11. KAUFMAN, V., RADZIEMSKI, L.J.Jr. and ANDREW, K.L., *J. Opt. Soc. Am.*, **56** (1966) 911.
12. HALL, T.C. and BLACET, F.E., *J. Chem. Phys.*, **20** (1952) 1745.
13. VERHOEK, F.H. and DANIELS, F., *J. Am. Chem. Soc.*, **53** (1931) 1250.
14. ACKERMAN, M., *Aeronomica Acta A n° 77* (1970) in : Fiocco, G. (ed.). *Mesospheric Models and Related Experiments*, Reidel Pub. Cy., Dordrecht-Holland, 1971, p. 149.
15. JOHNSTON, H.S., CIAP 72-4 Newsletter, December 8, 1972.
16. KOCKARTS, G., *Aeronomica Acta A n° 78* (1970) in : Fiocco, G. (ed.). *Mesospheric Models and Related Experiments*, Reidel Pub. Cy., Dordrecht-Holland, 1971, p. 160.
17. KOCKARTS, G., *Aeronomica Acta A n° 107* (1972).
18. NICOLET, M., *Ann. Geophys.*, **26** (1970) 531.
19. NICOLET, M., *Aeronomica Acta A n° 79* (1970) in : Fiocco, G. (ed.). *Mesospheric Models and Related Experiments*, Reidel Pub. Cy., Dordrecht-Holland, 1971, p. 1.